Lattice dynamics and thermal expansion behavior in the metal cyanides MCN (M = Cu, Ag, Au): Neutron inelastic scattering and first-principles calculations

M. K. Gupta,[1] Baltej Singh,[1] R. Mittal,[1] S. Rols,[2] and S. L. Chaplot[1]
[1]*Solid State Physics Division, Bhabha Atomic Research Centre, Mumbai 400085, India*
[2]*Institut Laue-Langevin, 71 Avenue des Martyrs, CS 20156, 38042 Grenoble Cedex 9, France*
(Received 29 October 2015; revised manuscript received 29 March 2016; published 18 April 2016)

We report measurement of temperature dependence of phonon spectra in quasi-one-dimensional metal cyanides MCN (M = Cu, Ag, Au). *Ab initio* lattice dynamics calculations have been performed to interpret the phonon spectra as well as to understand the anomalous anisotropic thermal expansion behavior in these compounds. We bring out the differences in the phonon mode behavior to explain the differences in the thermal expansion behavior among the three compounds. The chain-sliding modes are found to contribute maximum to the negative thermal expansion along the "c" axis in the Cu and Ag compounds, while the same modes contribute to positive thermal expansion in the Au compound. Several low-energy transverse modes lead to positive thermal expansion in the a-b plane in all the compounds. The calculated Born-effective charges show that AuCN has a covalent nature of bonding, which results in least distortion as well as the least number of unstable modes among the three cyanides. This result is well correlated with the fact that the coefficient of negative thermal expansion along the c axis in AuCN is the smallest.

DOI: 10.1103/PhysRevB.93.134307

I. INTRODUCTION

The phenomenon of large negative thermal expansion (NTE) in ZrW_2O_8 over a wide range of temperatures has led to extensive research [1–17] in this area since the last two decades. In fact, the phenomenon was observed long ago in water. The polyhedral framework compounds with large open structure are mostly found to exhibit this phenomenon, e.g., ZrV_2O_7, TaV_2O_5, $Sc_2(MoO_4)_3$, HfV_2O_7, etc. The discovery of colossal thermal expansion behavior in metal cyanide compounds [15,18,19] has further accelerated the research in this field. The discovery of NTE has led to industrial applications of these compounds in various areas such as fiber optics, coatings, electronics, and mirror substrates to tooth fillings, etc.

Most of the compounds exhibiting negative thermal expansion behavior consist of rigid polyhedral units around metal ions. The polyhedral units are mutually connected via terminal oxygens. The terminal oxygen plays an important role in governing the thermal expansion behavior in such compounds. ZrW_2O_8 is a very popular compound in this category. It shows isotropic negative thermal expansion behavior from 0.3 to 1050 K. Its structure remains cubic up to 1050 K, however, there is an order-disorder transition around 450 K. The low-energy transverse phonon modes in the compound are found to be very anharmonic in nature, which leads to transverse displacement of oxygen and causes NTE in ZrW_2O_8 [20–23]. The other framework compounds such as ZrV_2O_7 and HfV_2O_7 also show similar behavior, although their structures are different than that of ZrW_2O_8. A number of experimental and theoretical studies have been performed on such compounds. These studies suggest that the transverse vibration of oxygen and distortions of polyhedron units are mainly responsible for negative thermal expansion.

In the case of M_2O (M = Ag, Cu, Au) [24–26] compounds, the metal ion M acts as a terminal atom to connect M_4O polyhedral and plays an important role in NTE behavior. The difference in the thermal expansion behavior in these compounds mainly arises due to the difference in nature of bonding. The phonon calculations show that NTE in oxygen mediated compound is mainly supported by the structure, i.e., open structure. However, in compounds where metal atoms play the role of terminal entity, the nature of bonding between metal atom and oxygen is also found to be important in governing the thermal expansion behavior.

Recently, metal cyanides have gained attention. $Zn(CN)_2$ was the first compound in this category [27]. The word "colossal" is used to emphasize the huge thermal expansion behavior of the compound. The structure consists of a tetrahedral framework of Zn connected with four cyanide units. The tetrahedral units are connected through CN, which provide the flexibility to bend the tetrahedra and results in NTE behavior. The isostructural cyanide $Cd(CN)_2$ also exhibits NTE behavior. The magnitude of the negative thermal expansion coefficient is found to be larger [17] in comparison to $Zn(CN)_2$. The first-principles calculations have been done to understand the difference in magnitude of the negative thermal expansion coefficient in these two compounds. The calculations shows that low-energy phonons in $Cd(CN)_2$ are more sensitive to pressure than in $Zn(CN)_2$. NTE has been explained in terms of rotations, translations, and deformations of $M(C/N)_4$ coordinated tetrahedral [28,29].

Recently, a number of Prussian blue analogs were also found to exhibit NTE, where the feature is attributed to metallophilic interactions [19,30,31]. The studies have been done to see the impact of metallophilicity on colossal positive and negative thermal expansion in a series of isostructural dicyanometallate coordination polymers [32,33]. The cyanide compounds are found to exhibit the phenomenon of negative linear compressibility. The c axis in $Ag_3Co(CN)_6$ is found to show NTE as well as negative linear compressibility [9,18,34–37] behavior. $KMn[Ag(CN)_2]_3$ shows extreme negative compressibility mediated by selective soft-mode frustration [38]. All these compounds show NTE behavior due to their polyhedral dynamics and include rotation and distortion. The compounds consist of polyhedra units connected via C ≡ N, and are known

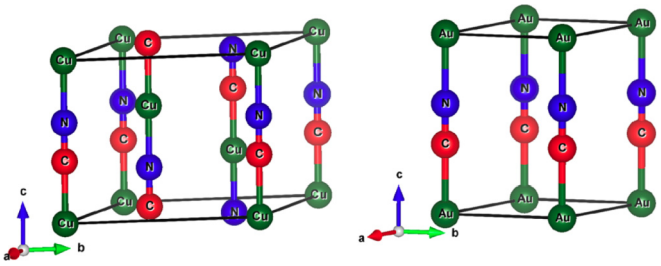

FIG. 1. The structure of AuCN and HT-CuCN/AgCN as used in the *ab initio* calculations. Key: C, red sphere; N, blue sphere; Cu/Ag/Au, green sphere.

to provide more flexibility in comparison to those where polyhedrals are connected via oxygens. It seems the structure consisting of $-C \equiv N-$ units provide much flexibility for the bending motion, which is found to be one of the major causes of NTE behavior in cyanides.

The thermal expansion behavior in low dimension MCN (M = Cu, Ag, Au) compounds shows anisotropic thermal expansion behavior. The structure of the compounds has been determined by various groups [10,39–44]. X-ray powder diffraction measurements have been performed [39] over a temperature range of 90–490 K. The structure of the cyanides is chainlike and resembles a quasi-one-dimensional structure. These chains consist of $C \equiv N$ units connected via metal ions ($M - C \equiv N - M$). The structure seems to be simple; however, the compounds show C/N disorder along the chain in terms of random flipping of C/N sequence. The higher dimension cyanides [17,45,46] such as $Cd(CN)_2$, $Ni(CN)_2$, and $Zn(CN)_2$ are also known to show C/N disorder behavior.

CuCN crystallizes in two different structures—named as low temperature and high temperature phase—at ambient condition depending on the method of synthesis. The low temperature (orthorhombic, $C222_1$) and high temperature (hexagonal, $R3m$) phases of CuCN in the paper are termed by LT-CuCN and HT-CuCN, respectively. The low temperature phase is a modulated structure of the high temperature phase. The modulation in LT-CuCN [44] is observed from previous neutron diffraction study. The structure of LT-CuCN consists of long $Cu-C \equiv N-Cu$ modulated chains, each containing five crystallographically distinct Cu atoms, which form a wave consisting of nine CuCN units.

At ambient condition, AgCN and HT-CuCN crystallize in the hexagonal $R3m$ (space group no. 160) cell. However, AuCN crystallizes in the $P6mm$ (space group no. 183) structure. The unit cell of AgCN and HT-CuCN consists of three formula units. However, the structure of AuCN consists of a single formula unit. All three compounds have three atoms in their primitive unit cell. The crystal structures as shown in Fig. 1 indicate that in AuCN all chains ($M - C \equiv N - M$) are parallel along to the c axis, while in HT-CuCN and AgCN the adjacent parallel chains are shifted by an amount of $c/3$ along the c axis.

Earlier reverse Monte Carlo simulations of the diffraction data have been performed to understand the local structure of these cyanides [39]. The buckling in the $M - C \equiv N - M$ chains is found [39] to increase with temperature. The magnitude of buckling is governed by the nature of bonding between the metal ions and the $C \equiv N$ unit. The analysis suggests that HT-CuCN has a large distortion perpendicular to the chain direction. Similar behavior is also observed in AgCN and AuCN; however, the magnitude of such distortion is very small in AuCN. The magnitude of distortion in all three compounds increases with temperature and is found to be correlated [39] with the thermal expansion coefficient along the chain direction (α_c). The thermal expansion coefficient is positive in the a-b plane; however, large NTE is found along the chain. The coefficient of negative thermal expansion along the chain direction for HT-CuCN, LT-CuCN, AgCN, and AuCN is $-27.9 \times 10^{-6}\,K^{-1}$, $-53.8 \times 10^{-6}\,K^{-1}$, $-14.8 \times 10^{-6}\,K^{-1}$, and $-6.9 \times 10^{-6}\,K^{-1}$, respectively [39,44].

Raman and infrared measurements have also been done [43] on MCN compounds. These measurements are limited to zone center, hence they do not provide complete information about the dynamics of the compounds. Here we present the temperature dependent inelastic scattering measurements on these cyanides. The measured spectra have contributions from all phonon modes from the entire Brillouin zone. Our studies provide vibrational properties of these cyanides, and an analysis of vibrational spectra using *ab initio* phonon calculations is useful to understand the thermal expansion behavior of these cyanides.

II. EXPERIMENTAL DETAILS

The polycrystalline samples of AgCN, AuCN, and LT-CuCN were purchased from Sigma Aldrich. The HT-CuCN was prepared by heating Aldrich supplied LT-CuCN for 2 hours under vacuum at 325 °C. The inelastic neutron scattering experiments on MCN (M = Cu, Ag, Au) were carried out using the IN4C spectrometers at the Institut Laue-Langevin, France. The spectrometer is based on the time-of-flight technique and is equipped with a large detector bank covering a wide range of about $10°-110°$ of scattering angle. The polycrystalline samples of MCN were prepared by the solid state reaction method. The inelastic neutron scattering measurements were performed at three temperatures from 150, 240, and 310 K. About 1 cc of polycrystalline samples of MCN have been used for the measurements. The low temperature measurements were performed using a helium cryostat. For these measurements we have used an incident neutron wavelength of 2.4 Å (14.2 meV) in neutron energy gain setup. In the incoherent one-phonon approximation, the measured scattering function $S(Q,E)$, as observed in the neutron experiments, is related [47–49] to the phonon density of states $g^{(n)}(E)$ as follows:

$$g^{(n)}(E) = A\left\langle \frac{e^{2W(Q)}}{Q^2} \frac{E}{n(E,T) + \frac{1}{2} \pm \frac{1}{2}} S(Q,E) \right\rangle, \quad (1)$$

$$g^{n}(E) = B \sum_k \left\{ \frac{4\pi b_k^2}{m_k} \right\} g_k(E), \quad (2)$$

where the $+$ or $-$ signs correspond to energy loss or gain of the neutrons, respectively, and where $n(E,T) = [\exp(E/k_BT) - 1]^{-1}$. A and B are normalization constants and b_k, m_k, and $g_k(E)$ are, respectively, the neutron scattering

TABLE I. The structure of various cyanides [42,58] ($T = 10$ K) as used in the calculations of phonon spectra. The "a" and "c" lattice constants and atom coordinates in the hexagonal unit cell are given.

	HT-CuCN($R3m$)	AgCN($R3m$)	AuCN($P6mm$)
a (Å)	5.912	5.905	3.343
c (Å)	4.849	5.291	5.098
V (Å^3)/Z	49.407	53.481	49.828
M (Cu, Ag Au)	1/3,2/3,1/3	1/3,2/3,1/3	0,0,0
C	1/3,2/3,0.714	1/3,2/3,0.724	0,0,0.387
N	1/3,2/3,0.952	1/3,2/3,0.942	0,0,0.613

length, mass, and partial density of states of the kth atom in the unit cell. The quantity between $\langle\rangle$ represents a suitable average over all Q values at a given energy. $2W(Q)$ is the Debye-Waller factor averaged over all the atoms. The weighting factors $4\pi b_k^2/m_k$ for various atoms in the units of barns/amu are 0.1264, 0.046 26, 0.039 44, 0.4625, and 0.8221 for Cu, Ag, Au, C, and N, respectively. The values of neutron scattering lengths for various atoms can be found from Refs. [50–52].

III. COMPUTATIONAL DETAILS

The *ab initio* phonon spectra can be calculated using either the supercell method or the density functional perturbation theory [53] method. We have used the former approach of supercell method to calculate the phonon frequencies. The PHONON software [54] is used to generate a supercell with various $(\pm x, \pm y, \pm z)$ atomic displacement patterns. The Hellman-Feynman forces on the atoms in the supercell have been calculated using density functional theory as implemented in the VASP software [55]. The phonon calculations for HT-CuCN, AgCN, and AuCN are performed considering the periodic lattice model using the experimental structure parameters [42,56] as given in Table I. The model is an approximation of the real situation where we have neglected the C/N disorder. The low temperature phase of CuCN is a modulated structure of the high temperature phase. The required supercell to perform the calculations makes it computationally very expensive. Our interest is to understand the differences in thermal expansion behavior in terms of vibration, elastic constants, and nature of bonding in these quasi-one-dimensional metal cyanide systems, hence we have performed a theoretical analysis on linear systems only.

There are three atoms in the primitive unit cell of the HT-CuCN, AgCN ($R3m$), and AuCN ($P6mm$) phases, which gives nine degrees of freedom. The nine displacement patterns are required to compute the phonon frequencies. For accurate force calculations we displaced the atoms in both the directions $(\pm x, \pm y, \pm z)$, hence the number of displacements is double (18). The energy cutoff is 580 eV and an $8 \times 8 \times 8$ k-point mesh has been used to obtain energy convergence in total energy of the order of meV, which is sufficient to obtain the required accuracy in phonon energies. The Monkhorst-Pack method is used for k-point generation [56]. The exchange-correlation contributions were approached within Perdew-Burke-Ernzerhof generalized gradient approximation [57]. The convergence criteria for the total energy and ionic forces were set to 10^{-8} eV and 10^{-5} eV Å^{-1}, respectively.

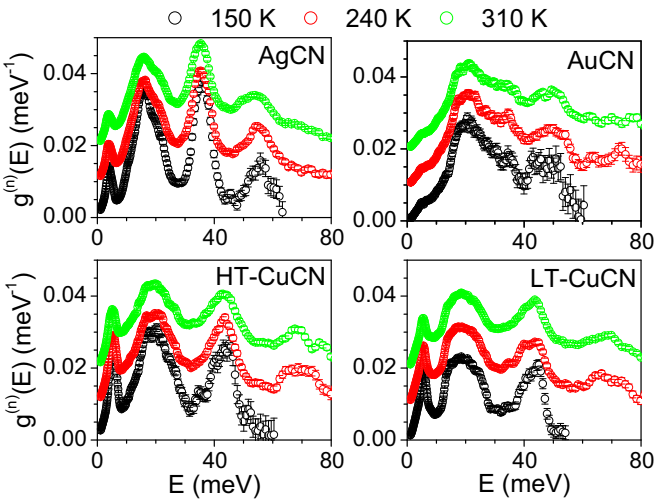

FIG. 2. The measured neutron inelastic spectra MCN (M = Cu, Ag, Au) at 150, 240, and 310 K.

The phonon spectra have been calculated in partially relaxed configurations, where only atomic coordinates are relaxed at fixed lattice parameters obtained from neutron diffraction data at 10 and 310 K [39,42,44,58].

The thermal expansion behavior has been computed under the quasiharmonic approximation. Each phonon mode of energy $E_{q,j}$ (jth phonon mode at point q in the Brillouin zone) contributes to the thermal expansion coefficient given by the following relation [59]:

$$\alpha_a(T) = \frac{1}{V_0}\sum_{q,j} C_v(q,j,T)[s_{11}\Gamma_a + s_{12}\Gamma_b + s_{13}\Gamma_c],$$

$$\alpha_c(T) = \frac{1}{V_0}\sum_{q,j} C_v(q,j,T)[s_{31}\Gamma_a + s_{32}\Gamma_b + s_{33}\Gamma_c],$$

where V_0 is the unit cell volume, and Γ_a, Γ_b, and Γ_c are the anisotropic mode Grüneisen parameters. In a hexagonal system, Grüneisen parameters $\Gamma_a = \Gamma_b$. The mode Grüneisen parameter of phonon energy $E_{q,j}$ is given as [59]

$$\Gamma_l(E_{q,j}) = -\frac{\partial \ln E_{q,j}}{\partial \ln l}; \quad l = a, c.$$

Here s_{ij} are elements of elastic compliances matrix $s = C^{-1}$.$C_v(q,j,T)$ are the specific-heat contributions of the phonons of energy $E_{q,j}$ and are given as

$$C_v(q,j,T) = E_{q,j}\frac{\partial}{\partial T}\left[\exp\left(\frac{E_{q,j}}{k_B T}\right) - 1\right]^{-1}.$$

The volume thermal expansion coefficient for the hexagonal system is given by

$$\alpha_V = (2\alpha_a + \alpha_c).$$

IV. RESULTS AND DISCUSSION

A. Temperature dependence of phonon spectra

We have measured (Figs. 2 and 3) the inelastic neutron spectra of MCN (M = Cu, Ag, Au) at 150, 240, and 310 K. As mentioned above, the measurements are carried out in the

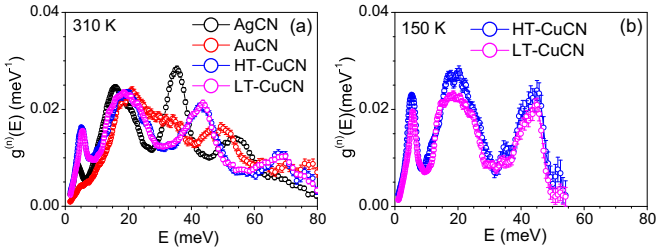

FIG. 3. (a) Comparison of the experimental phonon spectra for MCN (M = Cu, Ag, Au) at 310 K. (b) Comparison of the experimental phonon spectra for LT and HT phases of CuCN at 150 K.

energy gain mode which has allowed us to measure only the external modes. The C ≡ N stretching modes appear around 250 meV and would not be possible to measure due to the paucity of high energy phonons in the temperature range of the measurements. The phonon spectra of AgCN show peaks (Fig. 2) at about 4, 16, 36, and 55 meV. Further, we observe the peak about 36 meV soften with temperature. However, the peak at about 55 meV becomes more diffusive as the temperature increases from 150 to 310 K. The intensity of these peaks decreases as the temperature rises. The increase in temperature will enhance the vibrational mean square amplitude of atoms; hence the Debye-Waller factor would in turn reduce the intensity of the peaks.

Further, the measured spectra of AuCN show (Figs. 2 and 3) many broad features rather than sharp peaks as seen in the spectra of other compounds. The lowest peak is about 4 meV and the others peaks are observed around 20, 35, 50, and 75 meV. We could not observe any significant softening of phonon modes in AuCN with temperature.

However, in the case of HT-CuCN we observe (Figs. 2 and 3) that the lowest peak in the phonon spectra is at about 7 meV and other peaks are around 20, 45, and 70 meV. The lowest energy modes are shifted to high energies in comparison to AgCN. This could be partly due to the difference of mass of Cu (63.54 amu) and Ag (107.87 amu). We observe significant softening with temperature for phonon modes around 45 meV. The magnitude of softening in HT-CuCN is larger than that in AgCN.

In Fig. 3(b) we have shown the neutron inelastic scattering spectra measured at 150 K for high temperature and low temperature phases of CuCN. We find that the peak at around 20 meV in LT-CuCN seems to be broader in comparison to that in HT-CuCN, while at 300 K [Fig. 3(a)] the width of peaks in both the compounds seems to be the same. The larger width at low temperature in LT-CuCN may be due to the fact that the low temperature phase is a modulated structure of the high temperature phase. It seems that at higher temperature the effect due to the anharmonicity dominates and the inelastic spectra as measured in both the phases appear similar.

B. Calculated phonon spectra and elastic constants

The crystal structure of all three metal cyanides is known to show C/N disorder [39]. The C-N are randomly oriented along the c direction. The ideal structure of HT-CuCN and AgCN consists of chains of $-M-$CN$-M-$ along c axes. The

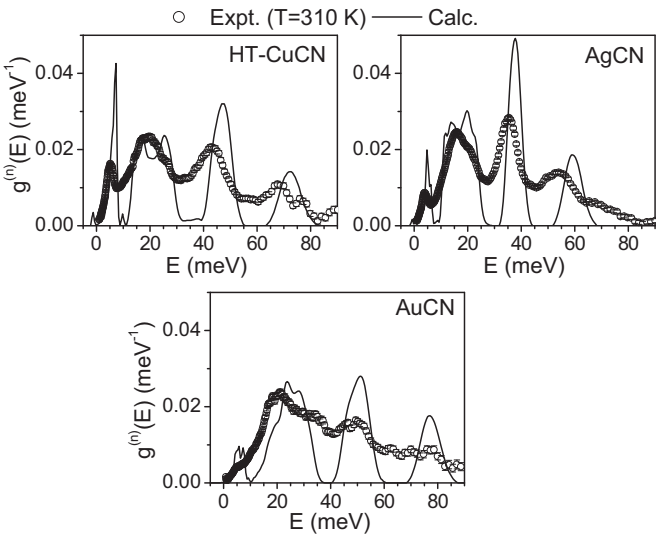

FIG. 4. The comparison between the measured (310 K) and calculated phonon spectra of MCN (M = Cu, Ag, Au).

ab initio phonon calculations are carried out considering the ordered structure of these compounds. We have calculated the phonon dispersion (Fig. 5) relation of all three compounds along various high-symmetry directions, namely, [100], [001], and [110]. We find that in all three compounds transverse acoustic modes along [001] are unstable. The mode involves transverse motion of C and N atoms in the a-b plane. The C/N disorder in the compounds might be responsible for stability of the crystal.

The comparison between the experimental and calculated phonon spectra is shown in Fig. 4. The calculated spectra are able to reproduce all the major features of the observed spectra. The structural disorder could lead to a variation of the $M-$C, $M-$N, and C$-$N bond lengths, which would in turn broaden the peaks as observed in the experimental spectra. This might be one of the reasons for the difference in the calculated and experimental spectra of MCN. We notice that for HT-CuCN and AgCN elastic instability is observed along [100] and [110]. However, for AuCN these modes are found to be stable. The slopes of the transverse acoustic phonon branches (Fig. 5) are very low. Hence, small errors in the calculation of phonon energies may result in large errors in the calculated elastic constants. So the elastic constants of MCN are calculated (Table II) using the symmetry-general least squares method [60] as implemented in VASP 5.2 and were derived from the strain-stress relationships obtained from six finite distortions of the lattice. The calculated elastic moduli include contributions of distortions with rigid ions and ionic relaxations. The elastic constants C_{11} and C_{33} are related to the longitudinal phonons polarized along the x and z axes. It can be seen that there is a large difference in the values of the C_{11} and C_{33} elastic constants in all the compounds. This indicates a large difference in the nature of bonding in the a-b plane and along the c axis. This is in agreement with the analysis of experimental diffraction data which also shows the strong one-dimensional nature of these compounds. The values of C_{33} for HT-CuCN, AgCN, and AuCN are 536, 387, and 755 GPa, respectively. The large value of C_{33} in AuCN

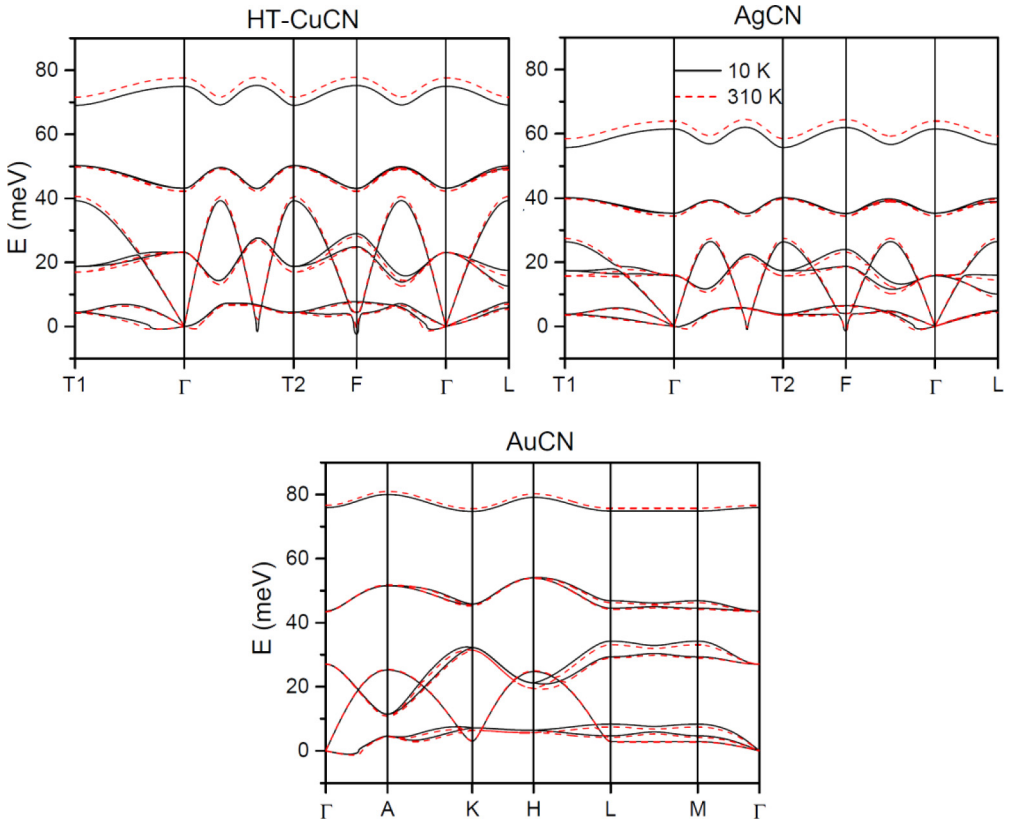

FIG. 5. The calculated dispersion relation along various high-symmetry directions of MCN (M = Cu, Ag, Au) at lattice constant at 10 K (black) and 310 K (red). The C-N stretching modes at about 270 meV are not shown. The Bradley-Cracknell notation is used for the high-symmetry points. HT-CuCN/AgCN: $T1(1/2,1/2,-1/2)_R \equiv (0,1,1/2)_H$, $\Gamma(0,0,0)_R \equiv (0,0,0)_H$, $T2(1/2,1/2,1/2)_R \equiv (0,0,3/2)_H$, $F(1/2,1/2,0)_R \equiv (0,1/2,1)_H$, $L(0,1/2,0)_R \equiv (-1/2,1/2,1/2)_H$; AuCN: $\Gamma(0,0,0)_H$, $A(0\,0\,1/2)_H$, $K(1/3,1/3,0)_H$, $H(1/3\,1/3\,1/2)_H$, $L(1/2\,0\,1/2)_H$, and $M(1/2,1/2,0)_H$. Subscripts R and H correspond to rhombohedral and hexagonal notation, respectively.

(∼ 755 GPa) in comparison to the other two compounds indicates that bonding between the atoms of −Au−CN−Au− chains is much stronger in comparison to that in Ag and Cu compounds.

The C_{66} elastic constant in all three compounds is very small. All these suggest that CuCN and AgCN are close to instability in plane against shear strain. However, the AuCN shows significant stability against the shear strain. On increasing temperature, the magnitude of strain arising due to the vibrational amplitude of atoms perpendicular to the chain will depend on the bond strength of $-M-$CN$-M-$. The calculated elastic constants as given in Table II indicate that the nature of bonding in AuCN is strongest among all three cyanides. This is consistent with the reverse Monte Carlo analysis of the diffraction data, which indicates that AuCN does not show any shear distortion even up to 450 K; however, significant distortion is observed in HT-CuCN and AgCN.

TABLE II. The various elastic constants and bulk modulus of metal cyanides MCN (M = Cu, Ag, Au) in units of GPa at $T = 0$ K.

	C_{11}	C_{33}	C_{44}	C_{66}	C_{12}	C_{13}	B
HT-CuCN	14.0	536.0	4.0	0.4	6.1	11.0	10.1
AgCN	18.5	387.0	5.2	−0.3	8.1	16.0	13.3
AuCN	28.4	755.3	6.5	2.2	15.3	14.0	21.8

C. Partial phonon density of states

The partial density of states provides the contributions of the individual atoms to the total phonon spectra. We have calculated (Fig. 6) the partial density of states by projecting the eigenvector on different atoms. The contribution from M (Cu, Ag, Au) atoms is spread up to 35 meV; however, it is a most significant contribution only below 10 meV. The C and N atoms contribute in the entire energy range up to 280 meV. We observed a band gap in the phonon spectra from 80 to 280 meV. The CN stretching modes are at around 280 meV. The low-energy peak in the partial density of states of Cu (63.54 amu), Ag (107.87 amu), and Au (197.97 amu) are at 7, 5.2, and 5.2 meV, respectively. The shift in the peak position is partly due to the mass renormalization. It should be noted that volume per primitive cell of HT-CuCN and AuCN compounds is nearly the same at 49.41 and 49.82 Å^3, respectively. The lowest energy peak in the Au compound does not follow the mass effect. This indicates that the nature of bonding for the AuCN ($P6mm$) is stronger in comparison to HT-CuCN and AgCN (both in $R3m$). The difference in ionic radii of Cu (0.73 Å), and Au (1.37 Å) along with the similarity in volume per primitive cell of these compounds further supports the idea of difference in nature of bonding.

The partial contributions due to C and N atoms in the HT-CuCN (49.41 Å^3) and AgCN (53.48 Å^3) in the external

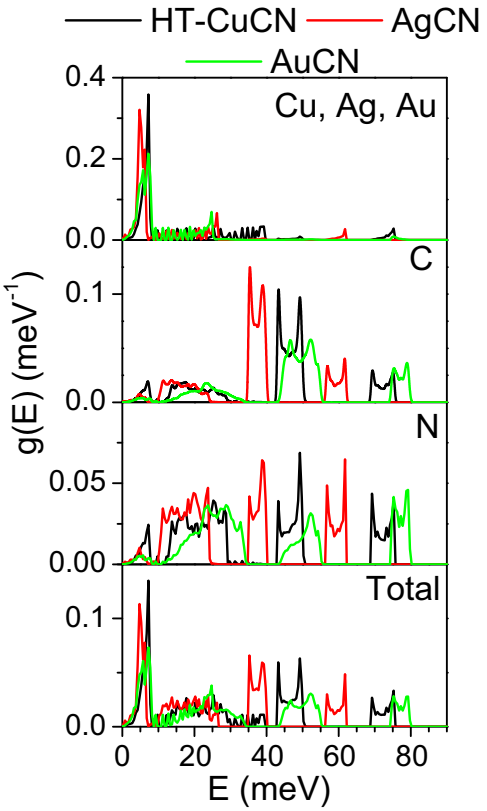

FIG. 6. The calculated phonon partial density of states of various atoms in MCN (M = Cu, Ag, Au) for structure at 10 K. The x scales of the C-N stretching modes at about 270 meV are not shown.

mode region (below 80 meV) are up to 75 and 62 meV, respectively. As expected, the difference in the energy range of the external modes in the two compounds seems to follow the volume effect. The volume of the primitive unit cell of AuCN is 49.82 Å^3. We find that external modes in AuCN extend up to 80 meV. Comparisons of the energy range of the external modes of the three compounds suggest that force constants are stiffer in AuCN in comparison to the other two compounds. The calculated C−N bond lengths (Table III) are 1.174, 1.169, and 1.163 Å in HT-CuCN, AgCN, and AuCN, respectively. As expected (Fig. 6) the energies of the phonon modes in the internal mode region simply follow the considerations due to change in C−N bond lengths. From the above analysis we can conclude that the nature of bonding along −Au−CN−Au− is stronger than that in −Ag−CN−Ag− and −Cu−CN−Cu−. This is consistent with the calculated Born-effective charges as discussed in Sec. IVD.

TABLE III. The various bond lengths in metal cyanides MCN (M = Cu, Ag, Au) in units of Å.

Bond length	HT-CuCN	AgCN	AuCN
C—N	1.174	1.169	1.163
C—M	1.841	2.040	1.960
N—M	1.835	2.081	1.976

In order to visualize the volume dependence of the phonon spectrum that is related to the implicit anharmonicity of phonons, we have calculated the partial density of states at the experimental [39] volumes at 10 and 310 K (Fig. 7). It can be seen that significant change in the phonon spectra with an increase in volume is observed in HT-CuCN and AgCN; however, in AuCN the change is not significant. The contributions due to the C and N atoms show large change around 45 and 75 meV in HT-CuCN and 35 meV and 60 meV in AgCN. In AuCN the spectral change of C and N is observed only around 80 meV. Interestingly, in the case of HT-CuCN the phonons around 35 meV soften with an increase in volume in contrast to 75 meV, which become harder. Similar behavior is also observed in AgCN for phonons of energy around 35 and 60 meV; however, the magnitude of anharmonicity seems to be different. The phonon of energies around 80 meV in AuCN harden with an increase in volume. The contributions of metal ions in phonon spectra are limited to low energies and the observed changes with volume are not very significant.

D. Born-effective charges

The computed Born-effective charges in all three compounds are listed in Table IV. We observe that the values of the charge of carbon, nitrogen, and M(Cu, Ag, and Au) atoms in all three compounds are different and anisotropic. This anisotropic behavior of the Born-effective charge suggests a difference in nature of bonding along a and c axes. We find that for M atoms the values of the Born-effective charges along the a axis are large in comparison to that along the c axis. However, for C and N atoms this trend is reversed. It is interesting to note that for the Cu and Ag compounds, the magnitude of Born-effective charges along the chain (c axis) has small finite value; however, in the Au compound the value is zero. This suggests a large difference in nature of bonding along the M−CN−M chain among various MCN. This could be due to the difference in electronegativity of Cu(1.9), Ag(1.93), and Au(2.54) atoms. The zero magnitude of the Born-effective charge for the Au compound along the c axis means that bonding along the chain may be either metallic or covalent. However, MCN are known to be insulators, hence the bonding between Au and CN may be covalent in nature.

Further for AuCN (Table II) the magnitude of C_{33} and C_{44} elastic constants, which are related to the longitudinal and transverse phonon frequencies along the c axis, is larger in comparison to the values for HT-CuCN and AgCN. This also suggests that the nature of bonding in AuCN is stronger in comparison to HT-CuCN and AgCN. The elements of the elastic compliances matrix $s = C^{-1}$ are given in Table V.

As discussed below in Sec. IVE, we have investigated the anharmonicity of phonons, which is strongly related to NTE, in terms of the nature of bonding and the variations among the three cyanides HT-CuCN, AgCN, and AuCN. The calculated Born-effective charges (Table IV) and elastic constants (Table II) are useful to correlate with the difference in nature of bonding which is in turn responsible for the difference in anharmonicity of modes and coefficient of NTE along the c axis in these compounds.

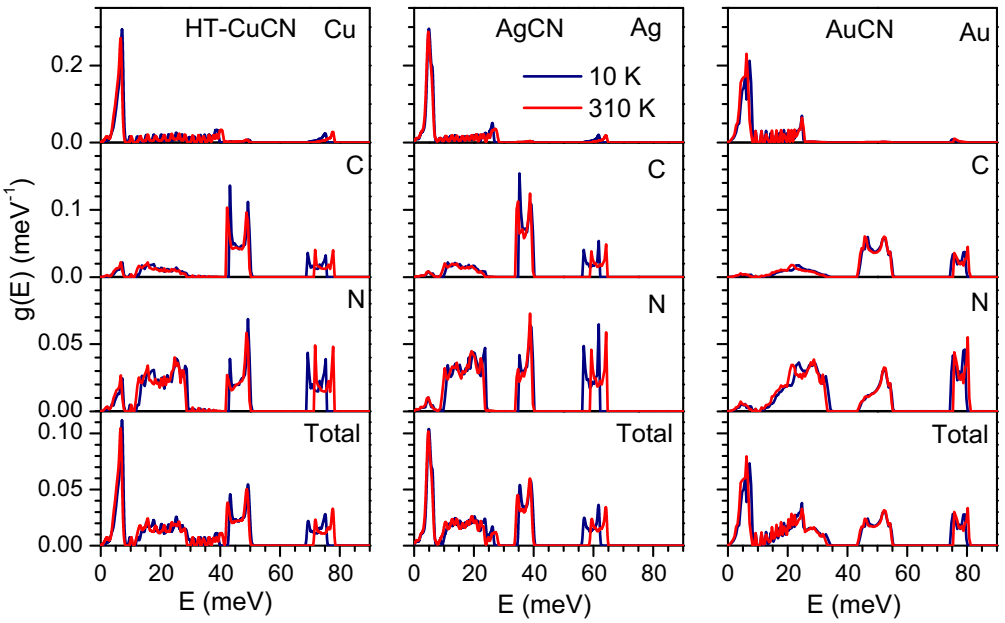

FIG. 7. The partial phonon density of states of MCN (M = Cu, Ag, Au) at structural parameters corresponding to 10 K (black) and 310 K (red). The x scales of the cyanide stretching modes at about 270 meV are not shown.

E. Thermal expansion behavior

The lattice parameter as a function of temperature has been reported from neutron diffraction measurements at temperatures ranging from 90 to 450 K [39]. The measurements show that the c lattice parameter decreases with an increase in temperature; however, lattice parameter $a(=b)$ shows positive expansion behavior. The overall volume thermal expansion is found to be positive in all three cyanides and has similar magnitude. The negative thermal expansion behavior along the c axis is largest in HT-CuCN and least in AuCN. So also, the positive expansion along the a and b axes is largest in HT-CuCN and least in AuCN. The phonon spectra in the entire Brillouin zone have been calculated at two volumes corresponding to the experimental structures at 10 and 310 K. It can be seen in Fig. 8(a) that the calculated Γ_a values for AuCN are significantly different than those calculated for HT-CuCN and AgCN. For AuCN, the low-energy modes below 5 meV have large positive values, while for the other two compounds these modes have small positive values. AuCN has large positive Γ_a values up to about 8 meV. The modes above 8 meV have small positive values of about 1.0. The calculated Γ_c shows that, for energies up to about 5 meV, all three compounds show large negative values (around -80). Above 5 meV, Γ_c values lie between $+10$ and -10.

The calculated partial density of states shows that the contribution at low energies at about 5 meV is mainly from the M(=Cu, Ag, Au) atoms. As shown in Fig. 5 the calculated transverse acoustic modes in HT-CuCN, AgCN, and AuCN are unstable. For the thermal expansion calculation the phonon energies have been calculated at 8000 q points (72 000 phonon modes) in the entire Brillouin zone. We find that among these 72 000 modes, the number of unstable modes in HT-CuCN, AgCN, and AuCN are 558, 453, and 75, respectively, which is less than 1%. The temperature dependence of the lattice parameters as well as unit cell volume is calculated without including the unstable modes.

Figure 9 shows the comparison between the calculated and experimental anisotropic thermal expansion behavior. It can be seen that the calculated negative thermal expansion behavior along the c axis in all three compounds is in good agreement with the available experimental data. As mentioned above, the *ab initio* calculations performed with the ordered structures exhibit the highest number of unstable modes for HT-CuCN, while AuCN shows the least number of unstable modes. The calculated Born-effective charges show (Table IV) that AuCN has covalent nature of bonding, which may result in the least transverse distortion as well as the least number of unstable modes, and also the coefficient of NTE along the c axis in AuCN to be the smallest [39] among the three compounds.

The calculated positive thermal expansion along the a axis is underestimated as compared to experiments in HT-CuCN and AgCN, while it is in good agreement with the observations in AuCN (Fig. 9). The underestimation in the calculated positive thermal expansion behavior along the

TABLE IV. The Born-effective charges of various atoms in units of e ($Z_{yy} = Z_{xx}$; $Z_{xy} = Z_{xz} = Z_{yx} = 0$).

Atom	Z_{xx}	Z_{zz}
C(HT-CuCN/AgCN/AuCN)	$-0.3/-0.4/-0.5$	1.4/0.8/1.5
N(HT-CuCN/AgCN/AuCN)	$-0.6/-0.6/-0.5$	$-1.1/-1.2/-1.5$
Cu/Ag/Au	0.9/1.0/1.0	-0.3/0.4/0.0

TABLE V. Calculated elastic compliance matrix components (s_{ij}) for metal cyanides MCN (M = Cu, Ag, Au) in GPa^{-1} units.

	s_{11}	s_{33}	s_{44}	s_{66}	s_{12}	s_{13}
HT-CuCN	0.093	0.002	0.500	12.300	−0.042	−0.001
AgCN	0.068	0.003	0.150	0.450	−0.028	−0.002
AuCN	0.050	0.001	0.200	−3.300	−0.027	0.000

a axis is responsible for considerable discrepancies in the volume thermal expansion behavior. The underestimation in the calculations is the maximum in HT-CuCN and least in AuCN. We argue that the underestimate might be related to the magnitude of transverse distortion in the $M-$CN$-M$ chains in these compounds. The total neutron diffraction data have been analyzed using the reverse Monte Carlo technique [39] which shows that the distortion in the $M-$CN$-M$ chain is least in AuCN. This distortion is found be disordered.

The experimental [39,44] value of the coefficient of NTE along the chain direction (α_c) for HT-CuCN, AgCN, and AuCN is $-27.9 \times 10^{-6}\,\mathrm{K}^{-1}$, $-14.8 \times 10^{-6}\,\mathrm{K}^{-1}$, and $-6.9 \times 10^{-6}\,\mathrm{K}^{-1}$, respectively, while positive thermal expansion (PTE) in the a-b plane (α_a) is $74.8 \times 10^{-6}\,\mathrm{K}^{-1}$, $65.7 \times 10^{-6}\,\mathrm{K}^{-1}$, and $57.4 \times 10^{-6}\,\mathrm{K}^{-1}$, respectively. As noted above, among the three compounds HT-CuCN has the highest distortion in the $M-$CN$-M$ chains and it has also the highest positive as well as negative thermal expansion coefficients. AuCN has the least $M-$CN$-M$ distortion and has the smallest values of NTE and PTE coefficients. It seems distortion stabilizes the structure and contributes towards positive thermal expansion behavior. The order-disorder transition at around 400 K in ZrW_2O_8 reduces [21] the overall NTE coefficient. It appears that the disorder contributes towards positive thermal expansion behavior. This was also found [46] in the case of nickel cyanide $Ni(CN)_2$ that has a large disorder along the c axis.

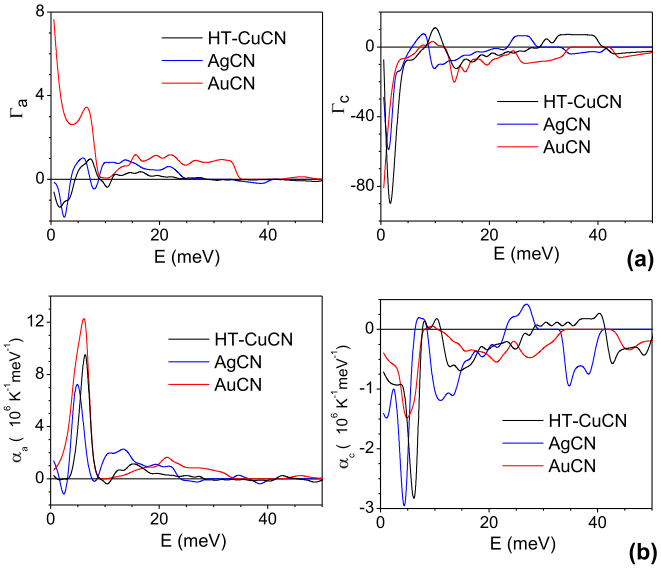

FIG. 8. (a) The calculated Grüneisen parameters (Γ_l, $l = a,c$) as obtained from anisotropic stress along the "a" and "c" axes. (b) The contribution of phonons of energy E to the linear thermal expansion coefficients (α_a and α_c) as a function of E at 300 K.

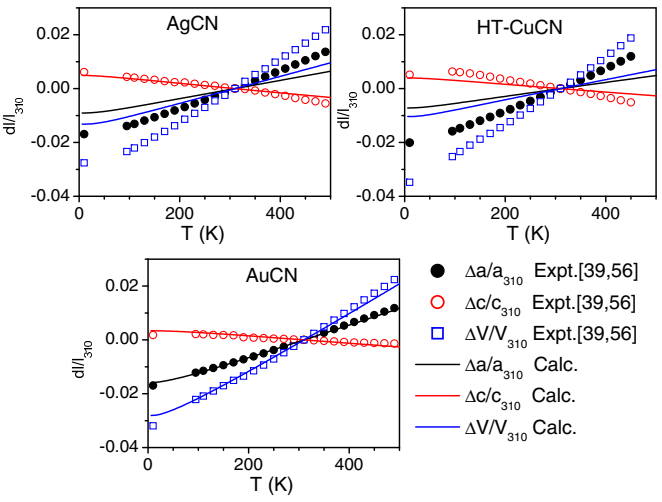

FIG. 9. The calculated and experimental thermal expansion behavior of MCN (M = Cu, Ag, Au).

As noted above, the linear thermal expansion coefficients along the "a" and "c" axes are found to be positive and negative, respectively. We are interested to find the modes which have large negative and positive Grüneisen parameters and contribute towards thermal expansion behavior. The estimated Grüneisen parameters (Γ_i) and the specific-heat contribution of modes (C_{Vi}) from the *ab initio* calculations have been used to estimate the contribution of the various phonons to the thermal expansion [Fig. 8(b)] as a function of phonon energy at 300 K. The maximum contribution to α_a and α_c seems to be from the low-energy modes below 10 meV. The calculated volume dependence of phonon dispersion curves for HT-CuCN, AgCN, and AuCN are shown in Fig. 5. The displacement pattern of a few zone-boundary phonon modes has been plotted (Fig. 10). The mode assignments, phonon energies, and Grüneisen parameters are given in the figures. As mentioned above, HT-CuCN and AgCN crystallize in the same space group ($R3m$); hence the eigenvector pattern for symmetrically equivalent phonon modes would be similar. The investigation of the displacement pattern of the eigenvectors shows that the phonon modes have mainly two kinds of dynamics. One kind involves atomic vibrations along the chain and the other in which atoms vibrate perpendicular to the chain.

For HT-CuCN and AgCN, the adjacent $-M-$C ≡ N$-M-$ chains are shifted by $\pm c/3$ along the c axis. We find that the lowest zone-boundary modes at the F and LD points in the Brillouin zone are found to be unstable. For the LD-point mode (Fig. 10), within a chain, the M and C ≡ N move with equal displacements. The movement of atoms in the adjacent chains is found to be out of phase with each other. The motion of the atoms in F-point mode is similar to that in the LD-point mode. However, for the F-point mode there is a small component of displacement in the a-b plane. Both the modes are found to become more unstable on compression of the lattice. Such type of modes would contribute maximum to the NTE along the c axis. However, in the case of AuCN, the K-point mode (Fig. 10) also shows sliding of $-M-$C ≡ N$-M-$

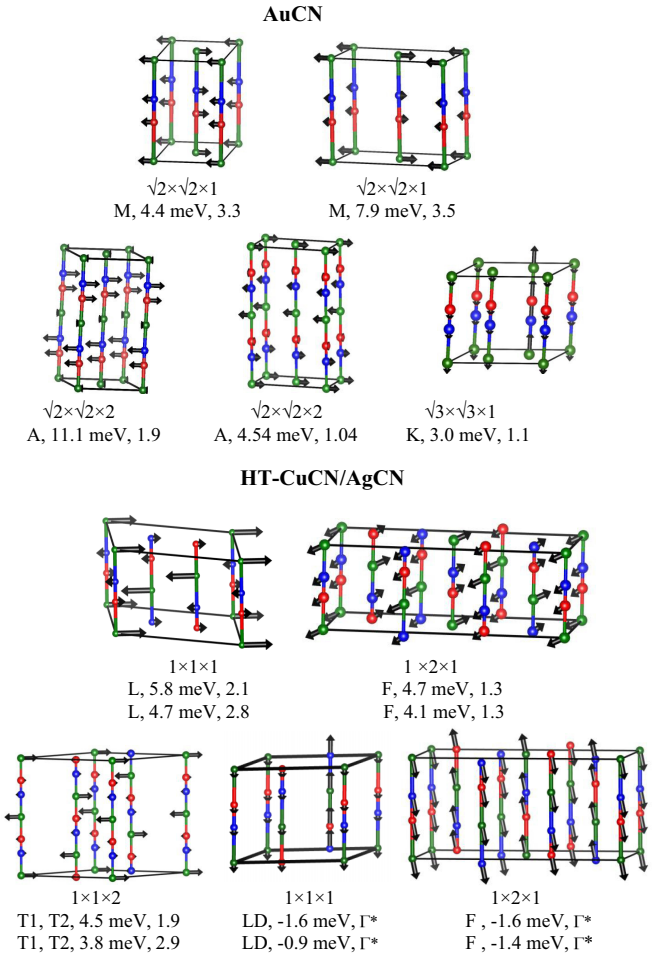

FIG. 10. The calculated displacement pattern of various phonon modes in AuCN and HT-CuCN and corresponding Grüneisen parameters. The first line below each figure represents the size of the supercell. The second line below the figure gives the high-symmetry point, phonon energies, and Grüneisen parameters, respectively. In the bottom panel (HT-CuCN and AgCN) the second and third lines below the figure correspond to HT-CuCN and AgCN, respectively. The Bradley-Cracknell notation is used for the high-symmetry points. AuCN: $A = (0\,0\,1/2)_H$, $K(1/3,1/3,0)_H$, and $M(1/2,1/2,0)_H$; HT-CuCN/AgCN: $L(0,1/2,0)_R \equiv (-1/2,1/2,1/2)_H$, $T1$, $T2(1/2,1/2,-1/2)_R \equiv (0,1,1/2)_H$, $F(1/2,1/2,0)_R \equiv (0,0.5,1)_H$, $LD(-2/3,1/3,1/3)_R \equiv (1,0,0)_H$. Subscripts R and H correspond to rhombohedral and hexagonal notation, respectively. The c axis is along the chain direction, while the a and b axes are in the hexagonal plane. Key: C, red sphere; N, blue sphere; Cu/Ag/Au, green sphere. *The Grüneisen parameter values of unstable F and LD-point modes are not given. The modes are found to become more unstable on further compression of the lattice. Such type of modes would contribute maximum to the NTE along the c axis.

chains out of phase with each other. The mode is found to have a small positive Γ of 1.1. It seems that the chain-sliding modes mainly contribute to negative α_c in the HT-CuCN and AgCN compounds and this contribution is not seen in AuCN.

The vibrational amplitude along the chain would depend on the nature of bonding between metal and cyanide ($-\mathrm{C} \equiv \mathrm{N}-$) as well as on the atomic mass of metal ion. As mentioned above, this bonding in HT-CuCN and AgCN seems to be similar. The smaller mass of Cu (63.54 amu) would lead to large amplitude of thermal vibration along the chain in comparison to the Ag (107.87 amu) compound, which indicates that the contraction along the $-M-\mathrm{C} \equiv \mathrm{N}-M-$ chain would be more in the HT-CuCN in comparison to the AgCN, which is qualitatively in agreement [39] with the observed NTE behavior in these compounds. Several modes in which the atoms move perpendicular to the chain have positive Grüneisen parameters and would be responsible for positive thermal expansion behavior.

V. CONCLUSIONS

We report a comparative study of the dynamics of quasi-one-dimensional metal cyanides MCN (M = Cu, Ag, Au) using inelastic neutron scattering measurements as well as through first-principles calculations based on the density functional theory. A good match between the calculated phonon density of states and that derived from inelastic neutron scattering measurements is obtained. The calculated anisotropic thermal expansion behavior is found to be in qualitative agreement with the available experimental data. We have also identified the specific nature of phonon modes associated with the sliding of $-M-\mathrm{C} \equiv \mathrm{N}-M-$ chains along the hexagonal axis and vibrations in the hexagonal plane, which are responsible for the anomalous thermal expansion behavior in these cyanides. The nature of the chemical bonding is found to be similar in HT-CuCN and AgCN, which is significantly different from a more covalent bonding in AuCN. The computed elastic constants and Born-effective charges are correlated with the difference in the nature of bonding and thermal expansion behavior in metal cyanides.

ACKNOWLEDGMENT

S.L.C. would like to thank the Department of Atomic Energy, India for the award of Raja Ramanna Fellowship.

[1] J. C. Hancock, K. W. Chapman, G. J. Halder, C. R. Morelock, B. S. Kaplan, L. C. Gallington, A. Bongiorno, C. Han, S. Zhou, and A. P. Wilkinson, Chem. Mater. **27**, 3912 (2015).

[2] M. S. Senn, A. Bombardi, C. A. Murray, C. Vecchini, A. Scherillo, X. Luo, and S. W. Cheong, Phys. Rev. Lett. **114**, 035701 (2015).

[3] L.-F. Huang, P.-L. Gong, and Z. Zeng, Phys. Rev. B **91**, 205433 (2015).

[4] J. Chen, L. Hu, J. Deng, and X. Xing, Chem. Soc. Rev. **44**, 3522 (2015).

[5] L. Wang, C. Wang, Y. Sun, K. Shi, S. Deng, H. Lu, P. Hu, and X. Zhang, J. Materiomics **1**, 106 (2015).

[6] V. J. Härkönen and A. J. Karttunen, Phys. Rev. B **89**, 024305 (2014).
[7] H. Fang, M. T. Dove, and A. E. Phillips, Phys. Rev. B **89**, 214103 (2014).
[8] F. Bridges, T. Keiber, P. Juhas, S. J. L. Billinge, L. Sutton, J. Wilde, and G. R. Kowach, Phys. Rev. Lett. **112**, 045505 (2014).
[9] P. Hermet, J. Catafesta, J. L. Bantignies, C. Levelut, D. Maurin, A. B. Cairns, A. L. Goodwin, and J. Haines, J. Phys. Chem. C **117**, 12848 (2013).
[10] J. Grant Hill, A. O. Mitrushchenkov, and K. A. Peterson, J. Chem. Phys. **138**, 134314 (2013).
[11] H. Fang, M. T. Dove, L. H. N. Rimmer, and A. J. Misquitta, Phys. Rev. B **88**, 104306 (2013).
[12] J. Hu and Y. P. Chen, Phys. Rev. E **87**, 062104 (2013).
[13] H. Fang and M. T. Dove, Phys. Rev. B **87**, 214109 (2013).
[14] V. Gava, A. L. Martinotto, and C. A. Perottoni, Phys. Rev. Lett. **109**, 195503 (2012).
[15] A. M. Chippindale, S. J. Hibble, E. J. Bilbé, E. Marelli, A. C. Hannon, C. Allain, R. Pansu, and F. Hartl, J. Am. Chem. Soc. **134**, 16387 (2012).
[16] T. Klimczuk, H. C. Walker, R. Springell, A. B. Shick, A. H. Hill, P. Gaczyński, K. Gofryk, S. A. J. Kimber, C. Ritter, E. Colineau, J. C. Griveau, D. Bouëxière, R. Eloirdi, R. J. Cava, and R. Caciuffo, Phys. Rev. B **85**, 174506 (2012).
[17] V. E. Fairbank, A. L. Thompson, R. I. Cooper, and A. L. Goodwin, Phys. Rev. B **86**, 104113 (2012).
[18] A. L. Goodwin, M. Calleja, M. J. Conterio, M. T. Dove, J. S. O. Evans, D. A. Keen, L. Peters, and M. G. Tucker, Science **319**, 794 (2008).
[19] K. W. Chapman, P. J. Chupas, and C. J. Kepert, J. Am. Chem. Soc. **128**, 7009 (2006).
[20] M. G. Tucker, A. L. Goodwin, M. T. Dove, D. A. Keen, S. A. Wells, and J. S. O. Evans, Phys. Rev. Lett. **95**, 255501 (2005).
[21] T. A. Mary, J. S. O. Evans, T. Vogt, and A. W. Sleight, Science **272**, 90 (1996).
[22] M. K. Gupta, R. Mittal, and S. L. Chaplot, Phys. Rev. B **88**, 014303 (2013).
[23] T. R. Ravindran, A. K. Arora, and T. A. Mary, Phys. Rev. Lett. **84**, 3879 (2000).
[24] M. K. Gupta, R. Mittal, S. L. Chaplot, and S. Rols, J. Appl. Phys. **115**, 093507 (2014).
[25] W. Tiano, M. Dapiaggi, and G. Artioli, J. Appl. Crystallogr. **36**, 1461 (2003).
[26] B. J. Kennedy, Y. Kubota, and K. Kato, Solid State Commun. **136**, 177 (2005).
[27] K. W. Chapman and P. J. Chupas, J. Am. Chem. Soc. **129**, 10090 (2007).
[28] D. Pei, E. J. Liang, J. Yu, and Z. Y. Du, J. Phys.: Condens. Matter **20**, 275224 (2008).
[29] J. W. Zwanziger, Phys. Rev. B **76**, 052102 (2007).
[30] S. Margadonna, K. Prassides, and A. N. Fitch, J. Am. Chem. Soc. **126**, 15390 (2004).
[31] A. L. Goodwin, D. A. Keen, M. G. Tucker, M. T. Dove, L. Peters, and J. S. O. Evans, J. Am. Chem. Soc. **130**, 9660 (2008).
[32] J. L. Korčok, M. J. Katz, and D. B. Leznoff, J. Am. Chem. Soc. **131**, 4866 (2009).
[33] A. L. Goodwin, B. J. Kennedy, and C. J. Kepert, J. Am. Chem. Soc. **131**, 6334 (2009).
[34] C. Mark, L. G. Andrew, and T. D. Martin, J. Phys.: Condens. Matter **20**, 255226 (2008).
[35] A. L. Goodwin, D. A. Keen, and M. G. Tucker, Proc. Natl. Acad. Sci. USA **105**, 18708 (2008).
[36] J. Catafesta, J. Haines, J. E. Zorzi, A. S. Pereira, and C. A. Perottoni, Phys. Rev. B **77**, 064104 (2008).
[37] A. L. Goodwin and C. J. Kepert, Phys. Rev. B **71**, 140301 (2005).
[38] A. B. Cairns, A. L. Thompson, M. G. Tucker, J. Haines, and A. L. Goodwin, J. Am. Chem. Soc. **134**, 4454 (2012).
[39] S. J. Hibble, G. B. Wood, E. J. Bilbe, A. H. Pohl, M. G. Tucker, A. C. Hannon, and A. M. Chippindale, Z. Kristallogr. - Cryst. Mater. **225**, 457 (2010).
[40] G. A. Bowmaker, B. J. Kennedy, and J. C. Reid, Inorg. Chem. **37**, 3968 (1998).
[41] S. J. Hibble, S. M. Cheyne, A. C. Hannon, and S. G. Eversfield, Inorg. Chem. **41**, 1042 (2002).
[42] S. J. Hibble, A. C. Hannon, and S. M. Cheyne, Inorg. Chem. **42**, 4724 (2003).
[43] C. Romao, M. M. Barsan, D. F. R. Gilson, and I. S. Butler, *A High-Pressure Raman Spectroscopic Study of the Negative Thermal Expansion (NTE) Behaviour of Some Cadmium(II) Cyanide Materials*, AIP Conf. Proc. No. 1267 (AIP, Melville, NY, 2010), p. 253.
[44] S. J. Hibble, S. G. Eversfield, A. R. Cowley, and A. M. Chippindale, Angew. Chem., Int. Ed. **43**, 628 (2004).
[45] D. J. Williams, D. E. Partin, F. J. Lincoln, J. Kouvetakis, and M. O'Keeffe, J. Solid State Chem. **134**, 164 (1997).
[46] A. L. Goodwin, M. T. Dove, A. M. Chippindale, S. J. Hibble, A. H. Pohl, and A. C. Hannon, Phys. Rev. B **80**, 054101 (2009).
[47] D. L. Price and K. Skold, *Neutron Scattering* (Academic, Orlando, 1986).
[48] J. M. Carpenter and D. L. Price, Phys. Rev. Lett. **54**, 441 (1985).
[49] S. Rols, H. Jobic, and H. Schober, C. R. Phys. **8**, 777 (2007).
[50] V. Correcher, Y. Rodriguez- Lazcano, J. Garcia- Guinea, and E. Crespo- Feo, Braz. J. Phys. **40**, 348 (2010).
[51] V. F. Sears, Neutron News **3**, 26 (1992).
[52] A. J. Dianoux and G. Lander, *Neutron Data Booklet* (Institut Laue-Langevin, France, 2002).
[53] S. Baroni, P. Giannozzi, and A. Testa, Phys. Rev. Lett. **58**, 1861 (1987).
[54] K. Parlinksi, PHONON 5.11 Software, 2003.
[55] G. Kresse and J. Furthmüller, Comput. Mater. Sci. **6**, 15 (1996).
[56] H. J. Monkhorst and J. D. Pack, Phys. Rev. B **13**, 5188 (1976).
[57] J. P. Perdew, K. Burke, and M. Ernzerhof, Phys. Rev. Lett. **77**, 3865 (1996).
[58] S. M. Cheyne, Ph.D. thesis, University of Reading, UK, 2004.
[59] E. Grüneisen and E. Goens, Z. Phys. **29**, 141 (1924).
[60] Y. Le Page and P. Saxe, Phys. Rev. B **65**, 104104 (2002).